

## Comparison of joint sets orientation in the Lower Paleozoic shales exposed in Scania (SW Sweden) and concealed in N Poland: a multi-methodological approach

Marcin OLKOWICZ<sup>1</sup>, \*, Kinga BOBEK<sup>1</sup>, Marek JAROSIŃSKI<sup>1</sup> and Radomir PACHYTEL<sup>1</sup>

<sup>1</sup> Polish Geological Institute – National Research Institute, Rakowiecka 4, 00-975 Warszawa, Poland



Olkowicz, M., Bobek, K., Jarosiński, M., Pachytel, R., 2021. Comparison of joint sets orientation in the Lower Paleozoic shales exposed in Scania (SW Sweden) and concealed in N Poland: a multi-methodological approach. *Geological Quarterly*, 65: 63, doi: 10.7306/gq.1632

Associate Editor: Piotr Krzywiec

The Lower Paleozoic shales of SW Sweden and Eastern Pomerania (Poland) have a common history related to the depositional and tectonic evolution of the Baltic Basin. The major tectonic events are recorded, among others, as joints, which are either exposed in outcrops in SW Sweden or recognised in deep boreholes located in Pomerania. We present a comparison of the regional joint systems recognized by multiple methods in the studied region. In effect of a statistical compilation of measurements, five joint sets (named JS 1 to JS 5) were identified, traceable between Eastern Pomerania and SW Sweden. Our analysis showed a general consistency of joint set orientations, independent of their distance to the Tornquist tectonic zone passing through the study region. Three of the joint sets, JS 1 striking NNE, JS 2 striking WNW, and JS 3 striking NNW, are found to be the most frequent sets, occurring in most sites. Having more constant orientation, the JS 1 and JS 3 served as indicators of possible rotation of the tectonic block or stress field in the region. JS 1 and JS 2 are interpreted as an effect of late Carboniferous stress relaxation after Variscan collision, while JS 3 and the E–W striking JS 4 might be related to the Early Devonian Caledonian compressive stage.

Key words: joint system, shale formations, Baltic Basin, photogrammetry, borehole scanner.

### INTRODUCTION

The most common serial fractures in sedimentary rocks form as joints, representing regional deformation, usually in scale of exposure and sometimes in boreholes they can be distinguished from the local fracture sets related to faulting (Gale et al., 2014). Joints occur in sets of relatively constant orientation over large areas, justifying the extrapolation of joint observations from a particular site to a larger scale. Spot borehole observations, enhanced by investigations of surface exposures, can allow recognition of the directions and frequency of joints on the scale of a sedimentary basin (Engelder et al., 2009, 2011). Individual joint sets behave more stably when the structural context is simple and the mechanical properties of the jointed formations are laterally homogeneous. These conditions often occur in low-deformed shale basins (e.g., the Baltic Basin), where claystone and mudstone facies are laterally uniform due to the calm deep-water sedimentation. In such formations joints

are generally well-developed and preserved. The compressive and tensional strength of most shales is relatively low, which facilitates rock failure via jointing (Zoback and Kohli, 2019). In shale, pore overpressure occurs very often due to low permeability, high susceptibility to compaction and a common increase in organic matter content, which produce overpressure by gas generation mechanism (Osborne and Swarbrick, 1997; Hill et al., 2004). Overpressure combined with tectonic stress changes controls development of joint sets. If the overpressure and tectonic factors have a regional scale, systematically oriented joints may develop that span the vast parts of shale basins along a range of hundreds of kilometres (Engelder et al., 2011). Systematic or sudden change of joint orientation may reflect regional changes in palaeostress.

Joint network and its characteristics are also key factors in shale gas exploration. Earlier studies of joint system in the Pomeranian part of the Baltic Basin were performed mostly within the framework of shale-gas projects based on borehole data (Bobek et al., 2017; Bobek and Jarosiński, 2018). However, borehole observations suffer from disadvantages related mostly to the limited volume of the investigated rock, unfavourable borehole geometry for analysis of sub-vertical fractures and high costs. Because of this, any additional data on joint network, especially based on accessible analogues of the area investigated, is valuable.

\* Corresponding author, e-mail: [marcin.olkowicz@pgi.gov.pl](mailto:marcin.olkowicz@pgi.gov.pl)

Received: March 30, 2021; accepted: December 14, 2021; first published online: December 31, 2021

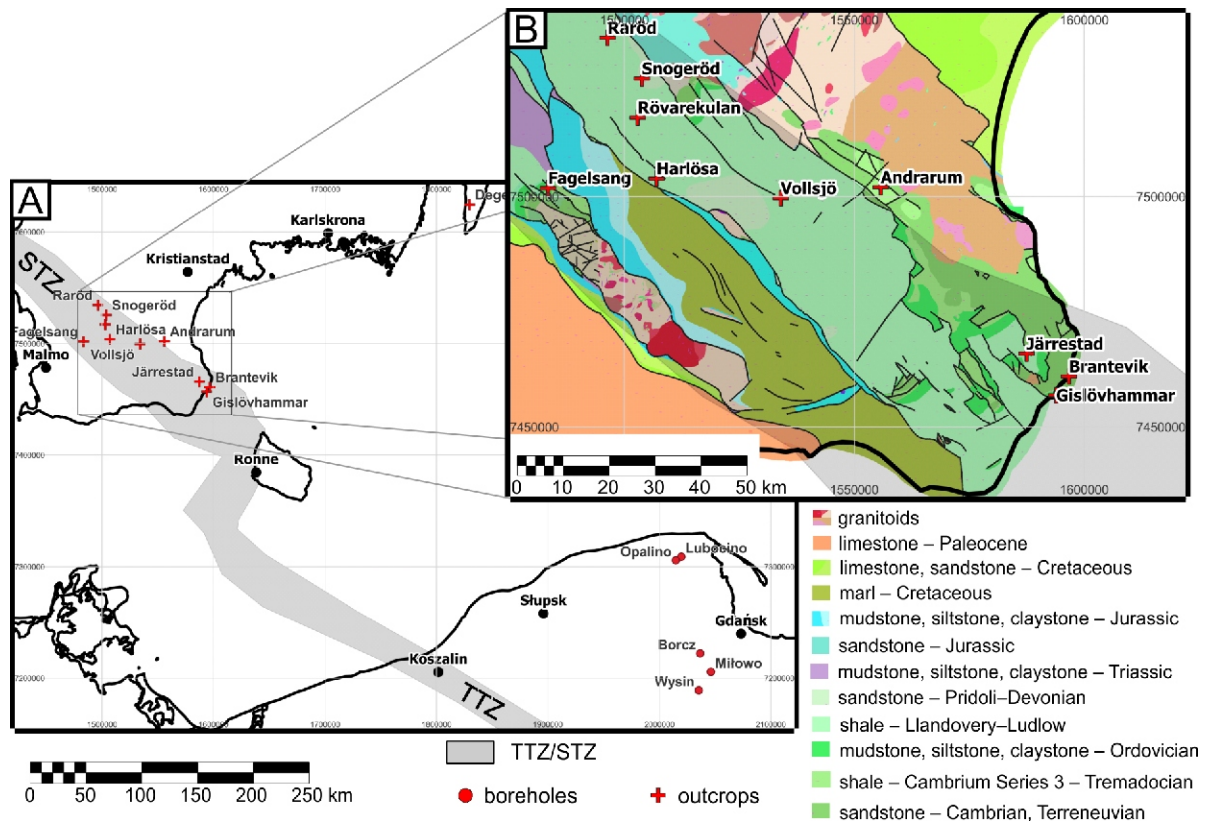


Fig. 1. Localization of boreholes in Pomerania (Poland) and exposures in Scania (Sweden)

Scania Geological map based on data provided by the Geological Survey of Sweden via <https://www.sgu.se>; **A** – overall view; **B** – Scania region in detail. STZ stands for the Sorgenfrei-Tornquist Zone, and TTZ for the Teisseyre-Tornquist Zone

For this reason, reconnaissance observations were conducted on exposures in Scania (Fig. 1). The Cambrian–Silurian formations of southern Sweden (Scania and Öland) are lithostratigraphically comparable to their equivalents in eastern Pomerania (e.g., Beier et al., 2000). Yet, there is a lack of joint system characterization for the Lower Paleozoic rocks of the Baltic Basin. The compilation of joint data from Scania and E Pomerania described in this study creates a starting point for more detailed analysis of the origin of a joint system at a more local scale. In this study we firstly describe joint sets orientations, using different methods of fracture detection and subsequently analyse joint sets in a different part of the basin, exploring reasons for changes in their orientation. In this way only the major changes of stress direction in the basin are considered. The detailed origin of the joints themselves needs separate studies focused on local constraints, such as burial history and hydrocarbon generation controlled by thermal events.

To collect the data from SW Sweden, the following methods were used: (1) classic, manual geological compass (GC) measurements made at exposures; (2) fracture trace analysis (TA) using satellite images provided by Google Earth; and (3) photogrammetrically constructed 3D digital outcrop models (DOM). This multimethod approach allows comparison of results, assessment of measurement repeatability and possible bias in data acquisition. The results obtained for the SW Sweden exposures were compared with a fourth data source, borehole observations from the Polish part of the Baltic Basin. The basin-scale scheme of the joint network is reconstructed based on the similarity of joint directions and the frequency of their occurrence at individual observation sites. The use of remote sensing and borehole logging approaches for fracture detection

do not allow constraints to be placed on the precise morphology of a fracture surface to infer its origin. Therefore, the results from remote sensing were compared with direct fracture observation at exposures or in borehole core, allowing, to some extent, control of character of fractures classified as joints.

We describe the fracture detection methods used, with detailed description of the photogrammetric approach. The results of joint orientations are shown separately for the sites where photogrammetric, satellite and compass measurements were made. For the rest the exposures in Scania where only compass measurements were performed, and for the boreholes from Pomerania, where the geophysical fracture record was interpreted, detailed descriptions are placed in appendices. Finally, the orientation of joint sets for the Baltic Basin was distinguished and compared between Scania and Pomerania. We also discuss the possible order of their genesis in the context of the Baltic Basin's evolution.

## GEOLOGICAL SETTING

The Lower Paleozoic strata of the area investigated, along with Bornholm, lithostratigraphically constitutes a part of the Caledonian foreland basin and its basement (Cocks and Torsvik, 2005). The entire study region (Scania, Öland and E Pomerania), starting from the early Cambrian to Mid-Ordovician, experienced slow marine sedimentation on the SW passive margin of the Baltica palaeocontinent (Calner et al., 2013). Mid-Ordovician to Upper Silurian/Lower Devonian deposits constitute the infill of the foreland basin developed in front of the North German–Polish Caledonides (Cocks and Torsvik, 2005),

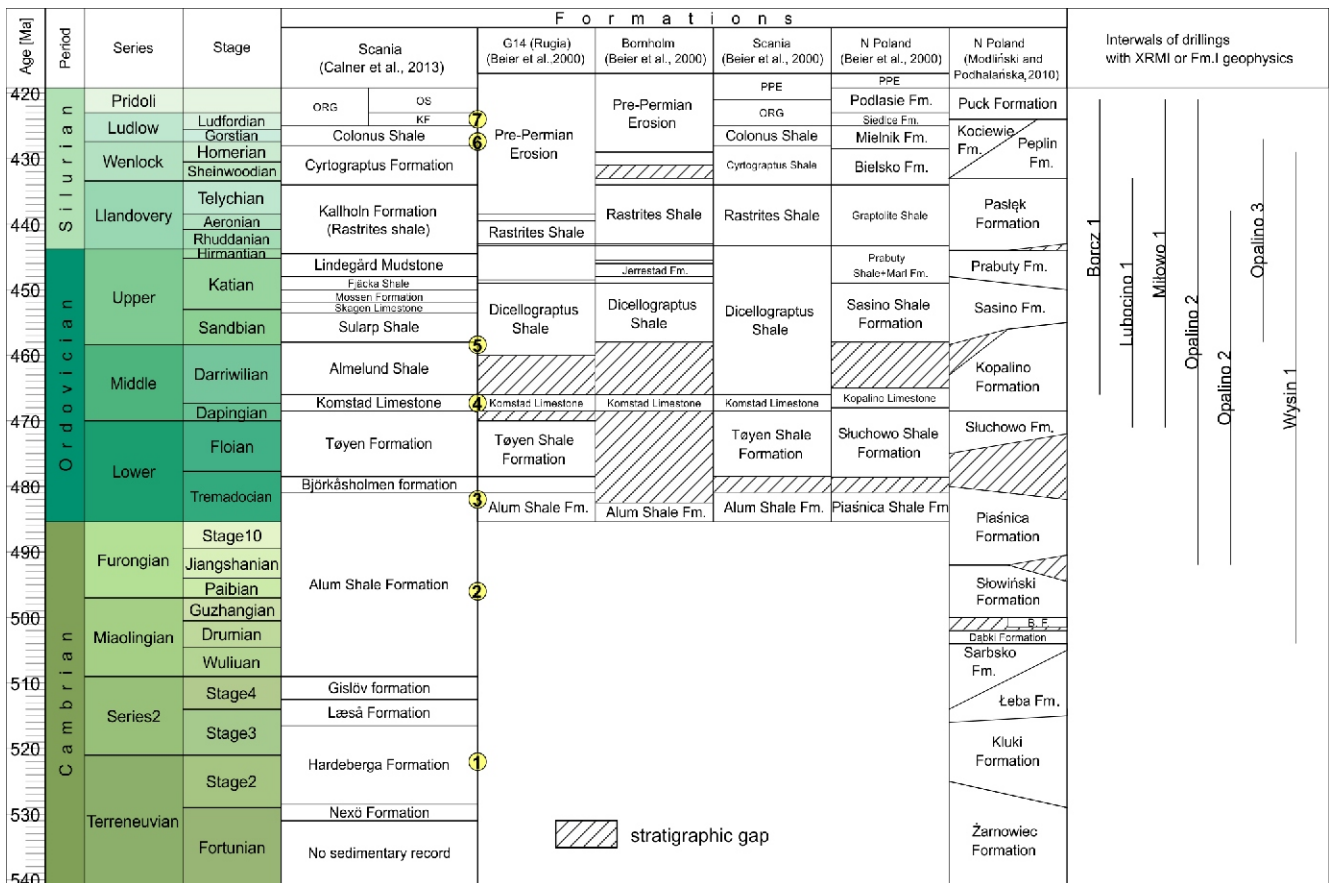


Fig. 2. Stratigraphic chart of the Lower Paleozoic for Scania, G14 offshore borehole NE of Rügen Island, Bornholm and N Poland

Based on Beier et al. (2000), Modiński and Podhalańska (2010), Calner et al. (2013). Yellow circles mark stratigraphic positions of outcrops in Scania: 1 – Brantevik; 2 – Andrarum; 3 – Degerhamn; 4 – Gislövhammar; 5 – Fågelsång; 6 – Järrestad, Rövarekulan, Vollsjö, Harlösa; 7 – Snogeröd, Råröd. The right-hand end shows the stratigraphic position of parts of N Poland (E Pomerania) including boreholes with XRFI or FMI geophysics. Unnamed formations were unnamed in the source works. ORG – Öved Ramsåsa Group; OS – Öved Sandstone; KF – Klinta Formation; PPE – Pre-Permian erosion; BF – Białogóra Formation

which stretches from Jutland in the west through Scania, Bornholm, N Poland, and farther east to Lithuania (Poprawa et al., 1999; Beier et al., 2000; Cocks and Torsvik, 2005). The regions investigated lie in two Confacies belts (Nielsen, 1995 after Jaanusson, 1976, 1982). Scania, Bornholm, and N Poland belong to the Scania Confacies Belt, and Öland to the Central Baltoscandian Confacies Belt. Therefore, these provinces show some differences in lithological development.

Comparing data from the Scania and Bornholm outcrops, the G14 well (located between Rügen and Bornholm), and boreholes drilled in E Pomerania, Beier et al. (2000) found that the sedimentation conditions were very similar across the entire area, and so most of the strata can be correlated lithostratigraphically (Fig. 2). Chronologically, the basin developed slightly earlier in the Scandinavian-German part than in N Poland due to the oblique, sinistral collision of Eastern Avalonia with Baltica (Poprawa et al., 1999; Poprawa, 2019). Beier et al. (2000) distinguished four major stages of the evolution of SW Baltica in the Paleozoic:

1. A pre-foreland basin phase, Lower Cambrian to lower Ordovician, related to deposition on the Baltica passive margin (Alum and Tøyen Shale in Sweden and their equivalents Piaśnica and Stuchowo Formations in E Pomerania).

2. An initial phase of foreland basin development, early to late Lanvirnian (late Dapingian–early Darriwilian), refers to the strong subsidence of the Baltica passive margin associated with thrusting of an accretionary wedge onto Baltica during the Caledonian Orogeny.
3. A deep water phase, late Lanvirnian (Darriwilian) to mid-Llandovery, starts with the Dicellograptus Shale and its equivalents (the upper Almelund Shale to Lower Lindegård Mudstone in Scania (Calner et al., 2013), the Sasino and Prabuty formations in E Pomerania) and continue to the Rastrites Shale (Kallholn Formation in Scania; Graptolite Shale and Pasłęk formations in N Poland; Fig. 2). During this basin starvation phase, subsidence was faster than deposition, and the foreland basin filled with deep water sediments containing bituminous shale.
4. A shallow water phase, late Telychian to Pridoli, reflects the effect of a distant accretionary wedge. During this phase, along with subsequent filling of the basin, the sedimentation rate exceeded subsidence, which resulted in a change of sedimentation regime from deep to shallow water. The basin depocenter migrated northwards from Bornholm to Scania. In N Poland, the shallow water phase started later than in the Scania-Ger-

many part of the basin. The phase starts with the Cyrtograptus Shale in Scania, followed by the Colonus Shale, and ends in the Öved Ramsåsa Group and their equivalents in E Pomerania: the Pelplin, Kociewie, and Puck formations (Modliński and Podhalańska, 2010). Recently, the youngest part of the Öved Sandstone was palynologically dated as of Lochkovian age (Mehlqvist et al., 2015).

The Lower Paleozoic of Öland (not included in Fig. 2) is represented by the Alum Shale overlain by the middle to upper Tremadocian Djupvik Formation and uppermost Tremadocian to Darriwilian limestones. Regarding the different development of Paleozoic formations in Öland, only the Alum Shale is lithostratigraphically directly correlated with the Piaśnica Formation.

A major tectonic structure in Scania and Bornholm comprises part of the Sorgenfrei-Tornquist Zone (STZ), which continues to the SE, where its Polish part is referred to as the Teisseyre-Tornquist Zone (TTZ). The Eastern Pomerania region, where the boreholes used in this study were drilled, covers an area NE of the TTZ, similarly to Öland located NE of the STZ. Outcrops of Lower Paleozoic strata in Scania are related to the Colonus Shale Trough (Erlstrom et al., 1997) bounded by major NW–SE striking faults (Fig. 1). The interior of the trough is cut by a system of minor NW–SE and NE–SW trending faults. The tectonic evolution of the STZ and TTZ, interpreted as an intracratonic fault zone (Franke, 1993; Mazur et al., 2015, 2020), is a sensitive marker of stress regime changes in the study area. Several tectonic stages were distinguished in the STZ by Erlstrom et al. (1997):

1. Cambro-Silurian: general subsidence of the region and fine-grained clastic and limestone sedimentation (thickness of sediments between 1–3 km) firstly on the passive margin of Baltica and secondly in the foreland of the Caledonian orogen; development of STZ and deep faulting. Mazur et al. (2015) suggested a Precambrian origin of the TTZ and only its overprinting by Caledonian tectonics.
2. Early Devonian: general uplift of the region and probable development of faults bordering the main tectonic elements.
3. Carboniferous: Variscan tectonic event dominated by dextral strike-slip NE–SW movements, which created downfaulted and tilted blocks by crustal transtension; Late Carboniferous and early Permian transtension (Thybo, 1997) associated with the intrusion of dolerite dyke swarms and volcanism in SW Sweden.
4. Mesozoic: reactivation of Paleozoic faults resulted in Late Triassic strike-slip movements with locally subsiding pull-apart basins; followed by late Jurassic minor normal faulting (Hansen et al., 2000; Bergerat et al., 2007); ending in a Late Cretaceous (Campanian–Maastrichtian) major inversion event (Erlström, 2020; Voigt et al., 2021) driven by Alpine collision, which resulted in transpressional uplift and erosion.
5. Cenozoic: a repetition of transpressional movements concurrently with phases of Alpine collision resulted in uplift and erosion in the Neogene. This, together with post-glacial isostatic rebound, resulted in the present-day surface arrangement of Lower Paleozoic strata.

## DATA AND METHODS

Due to limited access to the exposures, the basic measurements of fracture orientation across the outcrops made with a geological compass were supplemented by photogrammetric

measurements and analysis of satellite images. Fracture orientations were acquired from: 3D digital outcrop models (DOM) and geological compass (GC) measurements of SW Sweden shale exposures; satellite image of the island of Öland for trace analysis (TA) based on Google Earth Pro (GoogleEarth, 2020); and borehole logging data from E Pomerania provided by the Polish Oil and Gas Co.

## PHOTOGRAMMETRIC RECONSTRUCTIONS

Digital outcrop models (DOMs) constitute a well-established way to represent geological outcrops in 3D space (Bellian et al., 2005; Enge et al., 2007; Buckley et al., 2008). One of the most popular remote sensing methods for creating DOMs is photogrammetry (Sturzenegger and Stead, 2009; Assali et al., 2014; Bemis et al., 2014; Corradetti et al., 2017). In this study, the Structure from Motion (SfM) method (Jebara et al., 1999; Westoby et al., 2012) was used to build DOMs. This method allows reconstruction of the shapes and relative positions of modelled objects using a series of (at least 2) images taken from different camera positions.

During fieldwork, data for photogrammetric reconstructions were acquired with a Nikon D90 camera equipped with a Sigma 18–200mm f/3.5–6.3 lens. Photogrammetric reconstruction was performed using free software whose major components are SiftGPU (Wu, 2007), PBA (Wu et al., 2011), MVSC (Furukawa and Ponce, 2010), and VisualSfM (Wu, 2007). The reconstruction process results in the creation of a point cloud (PC), which discretely describes outcrops by points with x, y and z coordinates, along with an RGB triplet for each reconstructed point.

Processing of the SfM point cloud was performed in order to add appropriate reference (orientation in relation to the cardinal directions and proper scale) and enhance data quality. To do this, the following customized procedure was performed using Meshlab (Cignoni et al., 2008) and CloudCompare (CloudCompare, 2020) software:

1. Rescaling and reorientation – based on reference points measured in the field, a reconstructed model was rescaled to a 1:1 ratio and rotated according to the cardinal directions.
2. Initial filtering and segmentation – all background objects, vegetation, infrastructure and other relatively large unwanted regions were manually removed from the PC. Next, the PC was segmented into semi-equal area parts to improve the performance of further processing.
3. The main filtering (1) abnormally low point density regions were removed as outliers; (2) Poisson Surface Reconstruction was performed with low octree depth (7–8) to obtain the mean surface of the outcrop (M1). Next, a point cloud to mesh (PC to M1) distance was computed and all points with a distance greater than 2 times the standard deviation PC to M1 distances were removed. This allowed clearing of the PC from errors in the form of small point groups usually related to reconstruction errors or remaining patchy vegetation; (3) Poisson Surface Reconstruction was performed again with higher octree depth (10–11) to obtain a detailed surface of the exposure (M2). Finally, random points with known density (points/m<sup>2</sup>) were projected onto M2. This led to semi-equal spacing of points over the entire model, and hole filling with the interpolated surface (Fig. 3B, C).

Orientation measurements on a PC were taken using two methods. The first method was based on manual measurements, using the CloudCompare Compass plugin (Thiele et al., 2017); it can be described as a “point and click” procedure in

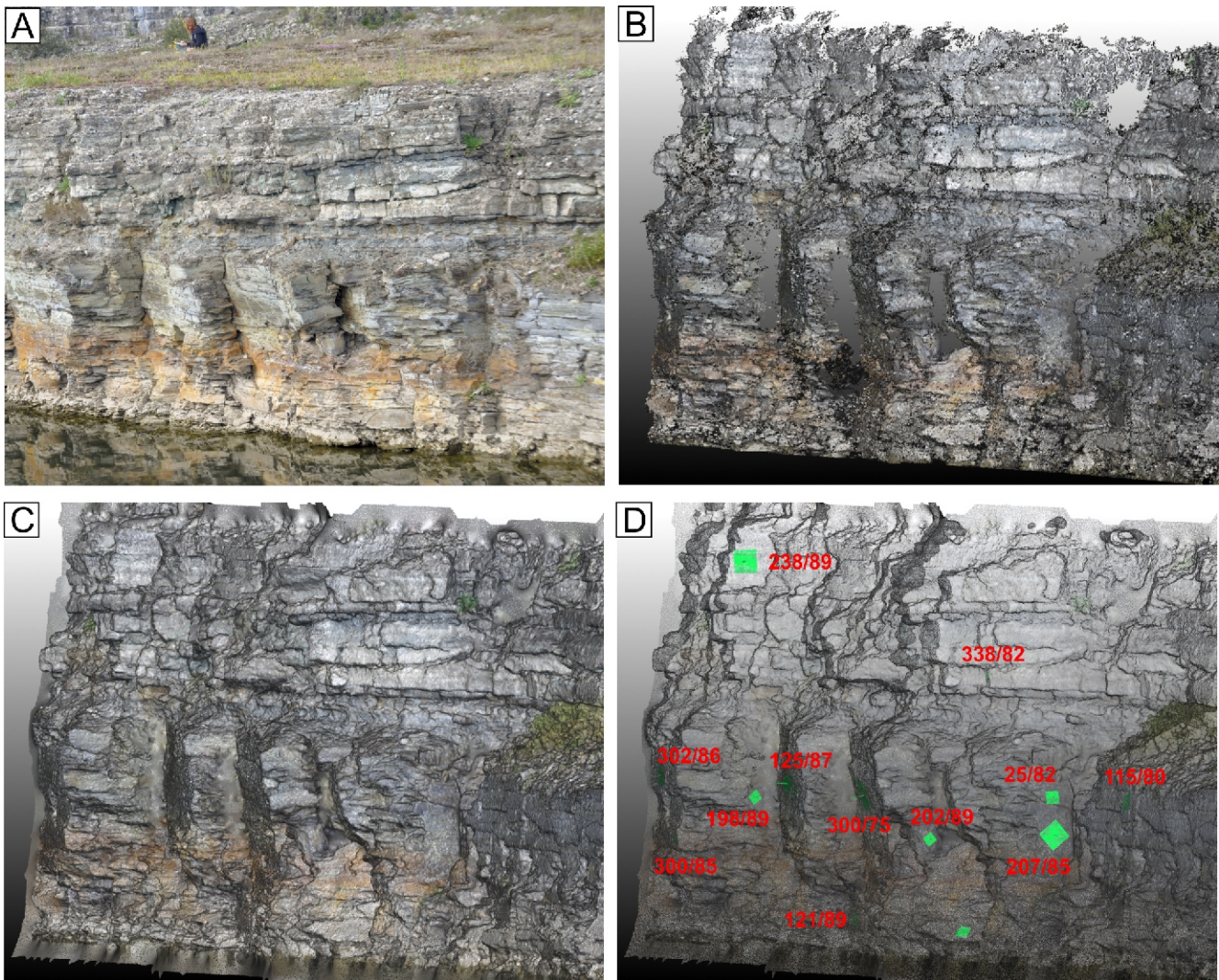


**Fig. 3.** Degerhamn Quarry, Öland, field image and DOM processing

**A** – example of an image used for photogrammetric reconstruction; **B** – raw 3D point cloud; **C** – point cloud after filtering (note filled holes and noise reduction); **D** – example of usage of the CloudCompare compass tool; green patches show surface measurements

which an operator decides where the measurement is taken (Fig. 3D). This relies on arbitrary decisions and thus can inherit human-related bias. The second method was to use the *CloudCompare Facets* plugin (Dewez et al., 2016) with a fast marching algorithm to automatically detect coplanar point cloud fragments (fracture surfaces). To improve fracture detection performance, previously filtered point clouds were used. According to field observations, mostly vertical or sub-vertical fractures were in the scope of interest. Thus, local surface orientation was computed and parts of the exposure characterized by a slope lower than  $40^\circ$  were removed from further analysis.

#### SATELLITE IMAGE ANALYSIS

The second data set on joint orientations comes from recognition of fracture traces on rectified aerial photographs. This method is often used to determine the spatial arrangement of fractures in 2D (Le Garzic et al., 2011; Bertrand et al., 2015; Samsu et al., 2020). Trace orientation analysis was performed in the area where the character of fractures could be largely observed. To record the strike of fractures, part of a well-exposed flat surface with visible fracture traces in the area of interest was

chosen using *Google Earth Pro*. Then, based on the exported image, fracture traces were manually digitized and recalculated to fracture strike. Since the satellite image has a limited resolution at the level of a few tens of centimetres, to avoid bias, only clearly identifiable structures, at least 10 metres long, were digitized as fracture traces. The results of fracture analysis were calibrated by field observations made in the nearby Degerhamn Quarry.

#### BOREHOLE LOG ANALYSIS

Joint orientations in the Lower Paleozoic shale of E Pomerania were interpreted from microresistivity image logs (Fig. 4A), while their character was assessed in borehole core (Fig. 4B). In this study, a combined length of 2123 m of Fullbore Formation Microlmager (FMI) and X-tended Range Microlmager (XRMI) scanner profiles were used. This analysis allowed the identification of 2675 joints with a minimum vertical extent varying from 2 cm to 9 m (Bobek and Jarošinski, 2021). The processing of raw logs was performed using Schlumberger's *TechLog* software. According to Brudy and Zoback (1999); Barton and Zoback (2002); Barton and Moos (2010);

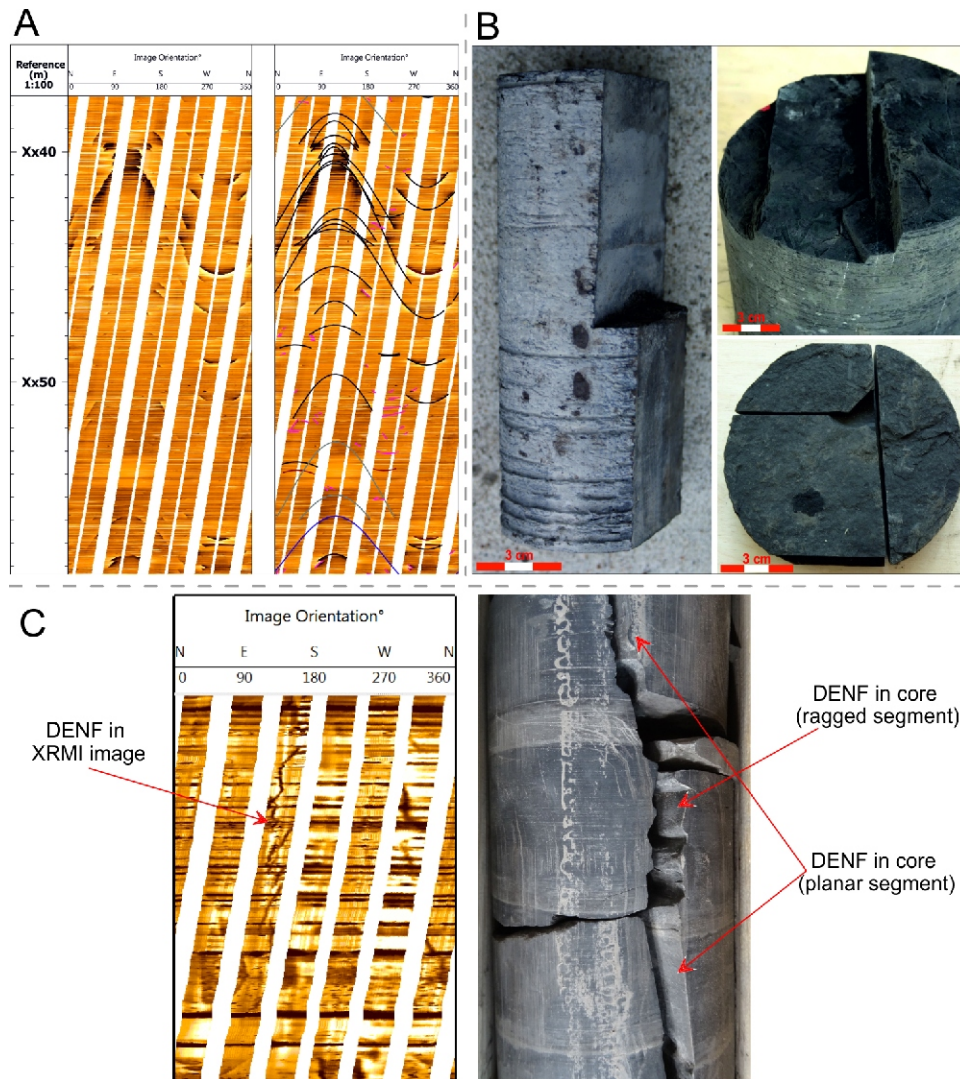


**Fig. 4. Fractures in borehole data**

**A** – fragment of Fullbore Formation MicroImager (FMI) log, sinusoidal lines indicate natural fracture traces; **B** – fractures observed in a borehole core; **C** – drill-enhanced natural fractures (DENF) in X-tended Range MicroImager (XRMI) log and borehole core

Nie et al. (2013), planar natural fractures in the microresistivity image should appear as sinusoidal traces (Fig. 4A) – brighter than the adjacent area if filled with calcite, and darker if open and filled with mud. However, within the boreholes investigated, the great majority of natural fractures are sub-vertical joints, which terminate at bedding planes and do not create the full sinusoidal intersection, but a pair of separate traces (Fig. 4A). The main difference between drill-induced fractures (DIF) and natural fractures, in this case, is the possibility of fitting a flexible sinusoid within the fracture trace in the image. DIFs are formed only within the narrow tensile region, form straight, vertical traces, and fitting a sinusoid within them is not possible (Barton and Zoback, 2002). Drill-enhanced natural fractures (DENF), the effect of reopening natural fractures parallel to the smallest horizontal stress (Nie et al., 2013), were observed as vertical ragged traces (Fig. 4C). To differentiate them from DIFs, corresponding fractures in drill core were inspected (Bobek and Jarosiński, 2018). To check the representativeness of the orientation of fractures acquired by the microresistivity imaging, the results were compared to core data from an oriented part of the borehole core (Bobek and Jarosiński, 2021). The results

obtained indicated only small discrepancies in fracture intensity calculated for core and microresistivity images caused by high TOC content, calcite infill of veins and “critical angle” (Bobek and Jarosiński, 2018).

#### DATA PROCESSING

Analysis of fracture orientation was done using Matlab software. The build-in clusterization algorithm based on angular distance between measured fractures was used to distinguish joint sets (JSs). The maximum allowed angular distance between joints in a single cluster was specified to 50°. For data sets where the effect of clusterization was uncertain (e.g., a cluster with 2 strong maxima), the maximum allowed angular distance was changed in a range of 40–60°. The criterion of minimum sample size for the cluster to be distinguished as a JS was specified to 10% of all observations at the site analysed. This criterion was omitted in specific conditions when: (a) the overall number of observations in the data set was low; (b) one of the clusters contains the majority of observations and simultaneously clusters smaller than 10% form clear maxima on the

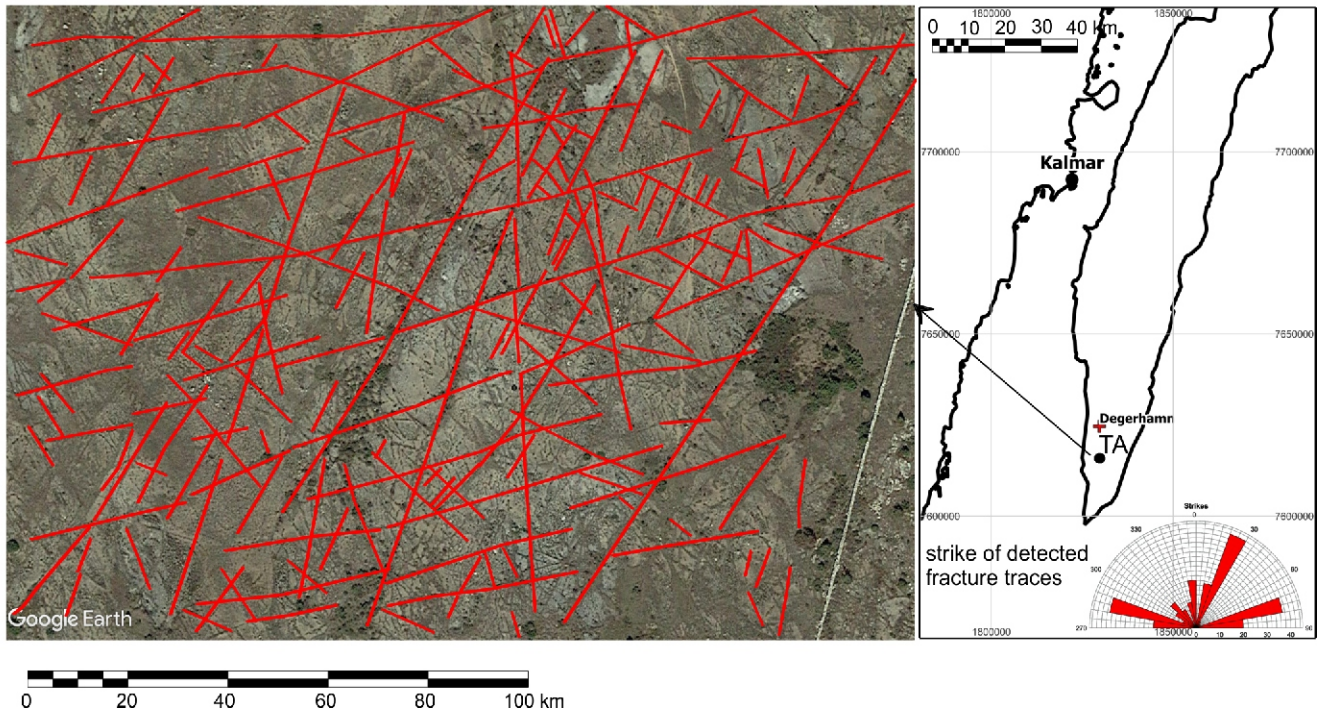


Fig. 5. Area near Degerhamn Quarry used for satellite image-based trace analysis

Fracture traces digitized as red lines

contour plot. Yet, in cases where one or both of these criteria were not met, a JS was considered uncertain. JS orientation was obtained by finding the maximum density of plane poles in the area that belonged to a cluster. The term “fracture cluster” or “cluster”, above and hereafter, is used to describe a group of similarly oriented fractures on a stereo plot, and not to refer to the spatial arrangement of fractures.

## COMPARISON OF MEASUREMENT METHODS

The rock exposure data was validated by comparing results obtained from different methods. Three tests based on comparison of DOM data, geological compass measurements (GC), and data from fracture trace analysis (TA) were performed. The tests were named T1 Andrarum, T2 Andrarum, and T3 Degerhamn according to their locations. Despite the usefulness of DOM-delivered data in structural analysis as demonstrated in many studies (Assali et al., 2014; Bemis et al., 2014; Corradetti et al., 2017; Jordá Bordehore et al., 2017; Klawitter et al., 2017; Menegoni et al., 2018), our tests do not yield comprehensive information about method validation. Instead, the tests were designed to assess the expected reliability of the DOM-based measurement and consistency with other methods in field conditions, specific to this work.

The first test (T1 Andrarum) aimed at direct fracture comparison between geological compass (GC) and DOM measurements performed on the Cambrian Alum Shale. At this location, fractures of different sizes, orientations, and states of preservation are present (some of them partially weathered), creating a wide spectrum of potential difficulties in applying the methodology described. The next two tests (T2 Andrarum and T3

Degerhamn) were performed to check the difference between measurements obtained from DOM by the Virtual Compass plugin, named “MANUAL DOM”, and the Facet plugin, named “AUTO DOM”. At the Andrarum site, measurements were collected on the same exposure walls for direct comparison of the methods tested. By contrast with T1 Andrarum, the T2 Andrarum test was performed at exposure scale, showing additionally the impact of a different approach to fracture plane identification. In the T3 Degerhamn test, GC measurements were taken on a different quarry wall (trending 340°) than those used for the DOM (wall trending 15°), in order to include larger-scale observations. Additionally, data from trace analysis (TA) was collected from a selected bedding surface of ~24 000 m<sup>2</sup> (Fig. 5) and compared to DOM and GC measurements. As the TA measurements do not give fracture dips, the dips of TA-detected JSs were assumed to be sub-vertical, as with analogous JSs in the nearby Degerhamn Quarry (Fig. 7). Since in T3 Degerhamn test each of used data sets cover slightly different location their comparison may be treated as indirect which mean it includes the impact of spatial changes in the fracture network and the exposure wall orientation.

In the text below, a simplified notation, with only strike azimuth, is used to describe joint sets orientations or cluster positions. The strike is converted to a 270–090° range, except for directions similar to E–W, for easier joint sets comparison. Measurements from the test are presented on (Table 1 and Fig. 6); for details of the tests results, see Appendix 1\*.

Summarizing the tests results, T1 Andrarum shows good repeatability of measurements with a mean absolute error of 3°. For Andrarum T2 and Degerhamn T2, the auto DOM measurement always gives the highest number of records, which may affect the importance of individual sets. In the case of

\* Supplementary data associated with this article can be found, in the online version, at doi: 10.7306/gq.1632

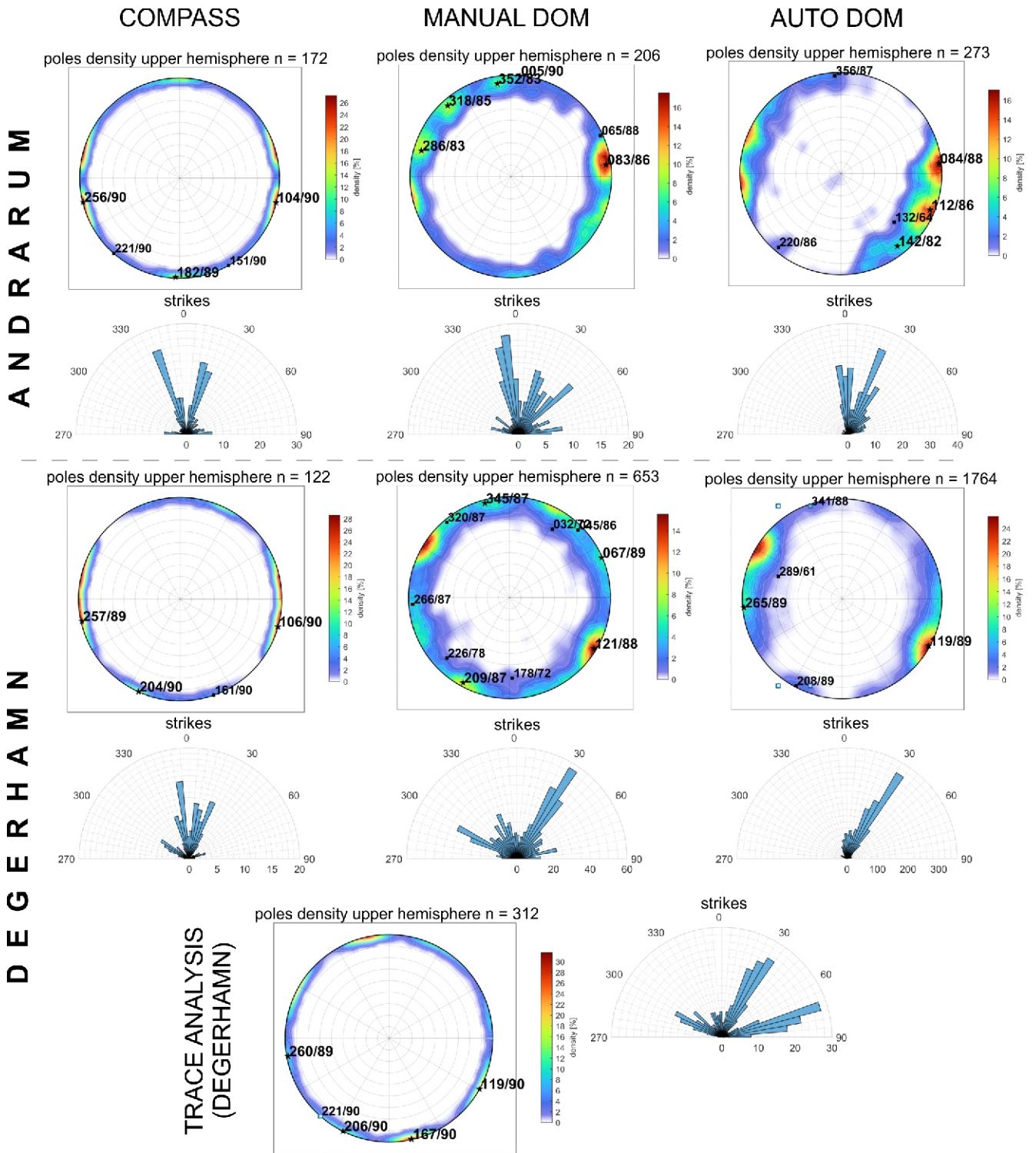


Fig. 6. Contour plots and rose diagrams of strikes from Andrarum and Degerhamm

COMPASS – measured with a geological compass in the field; MANUAL DOM – measurements taken on a DOM with Compass plugin; AUTO DOM – measurements taken on a DOM with Facets plugin; TA – Trace Analysis; JS – Joint Set; clusters with more than 10% of data marked with a pentagram, clusters with less than 10% of data marked with a square

Table 1

Major joint sets (detected fracture clusters) for the Andrarum and Degerhamn sites

Site	Data source	n	Major joint sets orientation [Strike/Dip Direction/Dip]*					Other sets
			JS 1	JS 2	JS 3	JS 4	JS 5	
Andrarum	GC	172	014/104/90	311/041/90 <sup>#</sup>	346/256/90 <sup>1</sup>	092/182/89	061/331/90 <sup>#</sup>	-
	Manual DOM	206	016/286/83	275/005/90 <sup>1</sup> 335/065/88 <sup>#1</sup>	353/083/86 <sup>1</sup>	082/352/83	048/318/85	-
	Auto DOM	273	022/112/86 <sup>1</sup>	310/220/86 <sup>#</sup>	354/084/88 <sup>1</sup>	-	052/142/82 <sup>1</sup>	042/132/64 <sup>#1</sup> 086/356/87 <sup>#1</sup>
	Mean		017/287/89	307/217/90	351/081/88	087/357/87	052/322/89	
Degerhamn	GC	122	016/106/90 <sup>1</sup>	294/204/90	351/077/90 <sup>1</sup>	071/161/90 <sup>#</sup>	-	-
	Manual DOM	653	031/121/88	299/029/87	337/067/89 356/266/87 <sup>#1</sup>	075/345/87	050/320/87 <sup>#</sup>	316/226/78 <sup>#1</sup> 358/178/72 <sup>#1</sup> 315/045/86 <sup>#1</sup> 302/032/72 <sup>#1</sup>
	Auto DOM	1764	029/119/89	298/208/90 <sup>#</sup>	355/265/89 <sup>1</sup>	071/341/88 <sup>#</sup>	-	019/289/61 <sup>#1</sup>
	TA	312	029/299/90	296/026/90	350/260/89	077/167/90	-	314/224/90 <sup>#</sup> 311/221/90 <sup>#</sup>
	Mean		026/116/89	297/027/90	349/259/89	073/343/89	050/321/86	

Unconventional notation of joint set orientation is used: Strike/Dip Direction/Dip. GC – joints measured with a geological compass in the field; Manual DOM – measurements taken on a DOM with Compass plugin; auto DOM – measurements taken on DOM with Facets plugin; TA – measurements from satellite trace analysis. # cluster grouping 1–10 % of plane poles; <sup>1</sup> – wide cluster with no clear maxima on a contour plot; \* – strikes converted to the range of 270–090, except for directions similar to E–W

Degerhamn, auto DOM gave almost 3 times more measurements than manual DOM. In auto DOM, due to the way the detection algorithm works, a single fracture may be measured multiple times on its different parts. For this reason, auto DOM measurements can be considered as weighted by area and coplanarity of exposed surfaces (for details see Dewez et al., 2016) and CloudCompare documentation (CloudCompare, 2020). Nevertheless, comparing measurement numbers from the DOM and GC shows how few fractures can be measured with a compass. It is also clear that in auto DOM interpretation one joint set may show a predisposed exposition and easily dominate over the rest of sets, blurring them. Because of this, for the auto DOM interpretation, it is crucial, in further analysis, to consider algorithm behaviour over the input point cloud. Test results show that the percentage of individual JSs in the total data varies depending on the method of fracture counting and detection used. This involves problems with wall exposition, fracture preservation, human bias, DOM quality, fracture size, and the various numbers of fractures counted. The differences found between the orientation of JSs detected from both DOM, TA and GC data are small compared to the observed JS width (span of measurements in a single JS), especially for “low fracture count” sets or sets with no clear maximum. Most observations between data sets are convergent. However, exploring the relation of the JS detection method to joint orientation, it does not matter which procedure of comparison, direct or indirect, was used, the variation of a single JS orientation can differ by up to 10° for clearly distinguishable fracture sets.

### FIELD DATA FROM SCANIA AND ÖLAND

Most field observations were taken on natural or artificial exposures that were not used for a long time, except for the relatively fresh walls in the Degerhamn Quarry. Due to mostly shale and mudstone lithologies in the exposures, quality of observation varies with both exposure preservation state (degree of shale weathering) and their size, which is reflected by the number of observations at individual exposures. For detailed descriptions of the Scania exposures see Appendix 2. The overall summary of exposure data is shown in Figure 7 and Table 2; for the Andrarum and Degerhamn contour plots, see Figure 6. In all data from SW Sweden, two joint sets are dominant, JS 1 (NNE) and JS 2 (WNW), being distinguished in 10 exposures. The third important joint set, JS 3 trending NW, was detected in 8 exposures. JS 4 trending E–W and JS 5 trending ENE were detected at five locations.

### BOREHOLE DATA FROM EASTERN POMERANIA

The length of a borehole interval covered by XRMI or FMI images varies from about 112 to 680 m (Table 3). Stratigraphically these intervals belong to the Lower Paleozoic, upper Cambrian to upper Silurian (Fig. 2). The location of the 7 boreholes analysed is shown in Figure 1. Due to their vertical orientation, the chance of detecting vertical fractures is low; however, several tens to hundreds of metres provide a statisti-

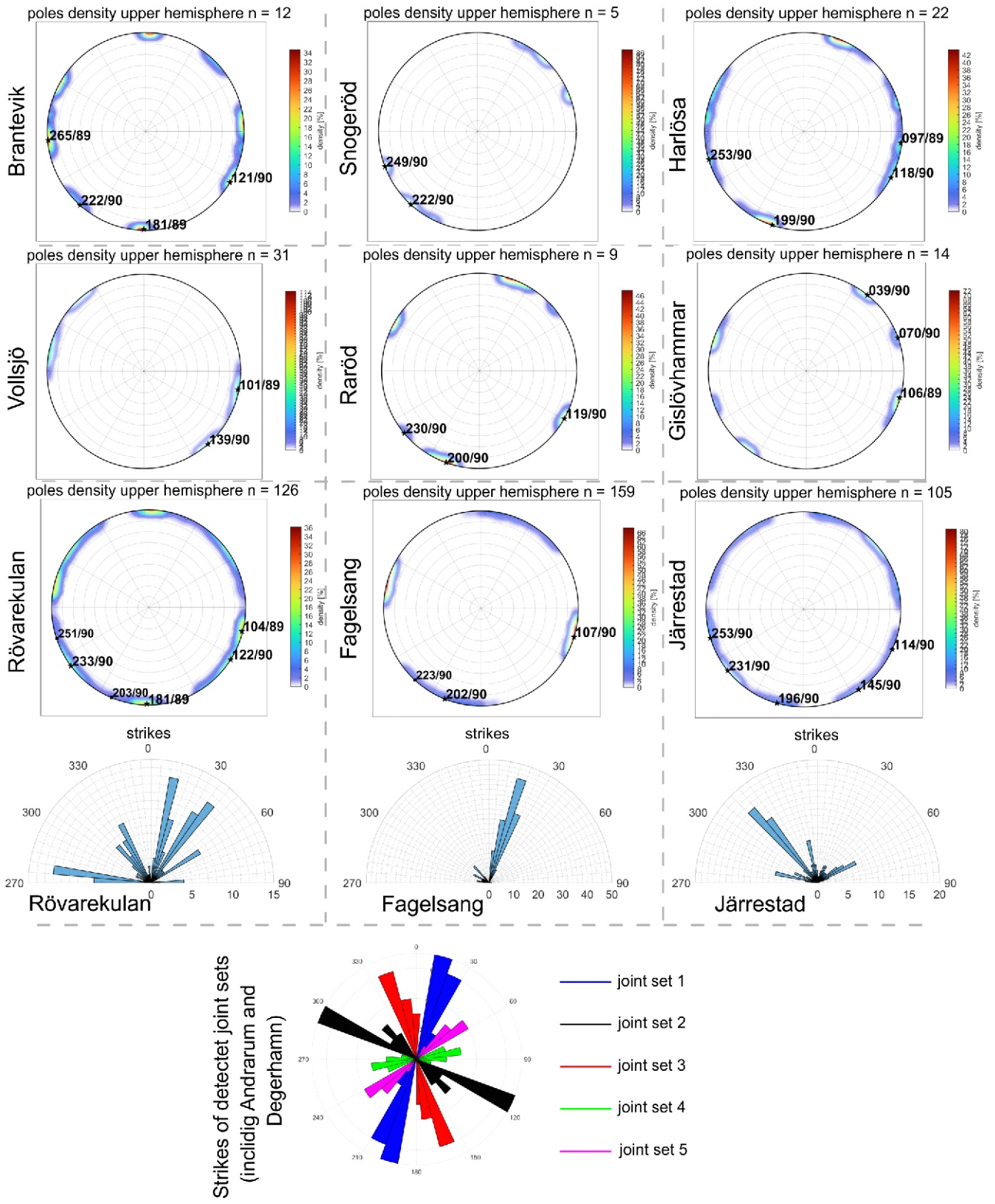


**Fig. 7. Fracture contour plots from Scania rock exposures based on GC measurements**

Rose diagrams of strikes for exposures with more than 100 fractures; clusters with more than 10% of data marked with a pentagram, clusters with less than 10% of data marked with a square; for Andrarum and Degerhamn see [Figure 6](#)

Table 2

**Major joint sets (detected fracture clusters) for the Scania exposures**

Site	n	Major joint sets orientation [Strike/Dip Direction/Dip]*					Other sets
		JS 1	JS 2	JS 3	JS 4	JS 5	
Brantevik	12	031/121/90	312/222/90	355/265/89	091/181/89	-	-
Snogeröd	5	-	312/222/90#	339/249/90#	-	-	-
Harlösa	22	028/118/90#	289/199/90	345/253/90	-	-	007/097/89#
Vollsjö	31	011/101/90	-	-	-	049/139/90	-
Råröd	9	021/111/90	290/200/90	-	-	-	320/230/90#
Gislövhammar	14	016/106/89	309/039/89	340/250/90	-	-	-
Rövarekulan	126	014/104/90	323/233/90?	341/071/90#	091/181/90	032/122/90	293/203/90#
Fågelsång	159	017/107/90	292/202/90	-	-	-	313/223/90#
Järrestad	105	024/114/90	321/231/90?	343/253/90	106/196/90	055/145/90	-
Andrarum (mean)		017/287/89	307/217/90	351/081/88	087/357/87	052/322/89	-
Degerhamn (mean)		026/116/89	297/027/90	349/259/89	073/0343/89	050/321/86	-
Mean		020/110/90	305/035/90	345/075/90	090/180/90	048/318/89	-

An unconventional notation of JS orientation is used: Strike/Dip Direction/Dip; \* – strikes converted to the range of 270–090, except for directions similar to E–W; # – uncertain observation (see [Appendices 1 and 2](#)); ? – observations with high deviation from the mean in JS

Table 3

**Major joint sets (detected fracture clusters) for E Pomerania boreholes**

Borehole	n	Major fracture sets orientation [Strike/Dip Direction/Dip]*					Other sets	Interval with XRMI / FMI
		JS 1	JS 2	JS 3	JS 4	JS 5		
Opalino 4	84	018/288/85	303/213/80	340/070/82	088/178/90	-	-	188 m
Opalino 3	254	016/106/85	293/023/73	-	-	043/133/77	315/045/77 001/091/63 048/158/81	143 m
Opalino 2	125	013/283/88	296/026/78	-	-	058/148/82	324/054/89	536 m
Wysin 1	50	017/287/90	291/021/73	339/069/85	082/352/90	061/331/80	310/220/70	160 m
Miłowo 1	1273	028/298/85	318/218/87	338/068/89	080/350/89	-	-	684 m
Borcz 1	714	025/115/84	291/021/87	336/066/88	-	048/138/87	-	301 m
Lubocino 1	94	025/295/89	303/033/89	342/072/89	079/169/88	-	291/021/64	112 m
Mean	-	020/290/89	299/029/84	339/069/86	082/172/90	053/143/86	-	-

An unconventional notation of JS orientation is used: Strike/Dip Direction/Dip; \* – strikes converted to the range of 270–090, except for directions similar to E–W

cally significant number of observations. As the scope of this work included only the sub-vertical fractures, there was no particular need to consider the influence of borehole orientation in JS detection. The detailed results of joint analysis of these boreholes are given in [Appendix 3](#).

The overall joint pattern is similar in all boreholes studied, showing three major sub-vertical JSs striking ~020°, 298° (in 7 boreholes) and 334° (in 5 boreholes) described as JS 1, JS 2, and JS 3, respectively ([Table 3 and Fig. 8](#)). Besides the main JSs, less developed JSs 4 and JS 5 were also observed in

some of the boreholes. No significant change of JS orientation was noticed with increase in depth or change in lithostratigraphic units. Two dominant joint sets occur in all boreholes: (1) JS 1, NNE-trending, clearly dominates in two boreholes, is well represented in another four boreholes, and poorly visible in one; (2) JS 2, WNW-trending, prevails in two boreholes, has a significant share in another three, and is subordinate in two, boreholes. In addition to these two sets, there is a subordinate JS 3, NNW-trending, which is well-developed in three boreholes, and poorly in another two. Other joint sets – JS 4 (E–W

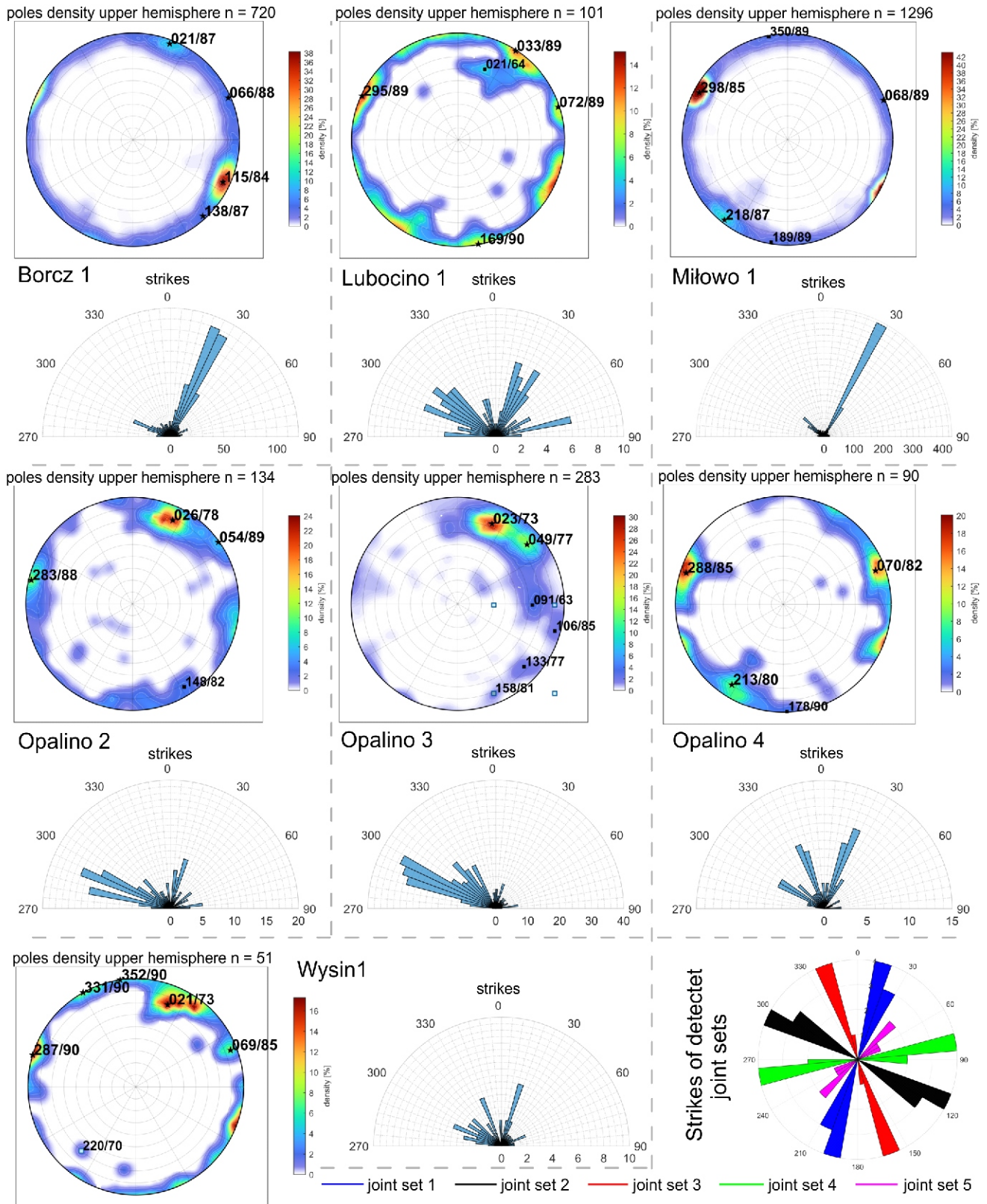


**Fig. 8. Fracture contour plots and rose diagrams of strikes from borehole XRMI and FMI data**

Clusters with more than 10% of data marked with a pentagram, clusters with less than 10% of data marked with a square

trending) and JS 5 (ENE-trending) – are clearly detectable in one borehole. JS 4 is also barely discernible in another four boreholes, and JS5 in three boreholes.

### JOINT SYSTEM OF THE BALTIC BASIN

A summary of measurement results reveals five joint sets (JS) of regional extent (Figs. 9 and 10), seen in both Scania and Öland exposures, as well as in E Pomeranian boreholes. Among these, JS 1 is the most frequently represented. It was identified at 17 sites (exposures and boreholes), and dominates at 8. JS 1 includes NNE-trending joints, which are characterized by a narrow range of orientation with an angular span of 20° and standard deviation of 6°. The mean joint directions of JS 1 in Scania and E Pomerania are the same with a mean strike of 020°. A second set of joints, trending WNW, JS 2, is also discernible at 17 sites. It dominates at 8 sites, characterized by a large angular spread of joint strike directions, which is 36° with a standard deviation of 11.5°. The mean trend of JS 2 in Scania is

slightly rotated clockwise, by 7° in relation to E Pomerania, but in Scania its angular span is noticeable bigger. JS 3, trending NNW, can be recognised at 13 sites. It dominates at only 2 sites, despite being relatively well-developed at 5. JS 3 has a moderate angular spread in a range of 19° and standard deviation of 4.8°. At exposure its angular span is the lowest of all the sets, within the range of 6°. Its mean direction in Scania is rotated by 5–7° clockwise with respect to E Pomerania. JS 4, trending E–W, was found at 9 sites, always subordinate, but well-developed at 7 sites. It has a large angular spread of joint orientation, reaching 35° with a standard deviation of 10°. For E Pomerania its span is more concentrated and ranges within 9°. Again, the mean joint trend in Scania is rotated clockwise in relation to E Pomerania. The last of the sets distinguished, JS 5, with NE-trending joints, was observed at 8 sites, among which it is well-developed at 4. It has a large scatter of joint directions, in the range of 29° with a standard deviation of 10°, while the rotation of these joints from E Pomerania to Scania is counter-clockwise.

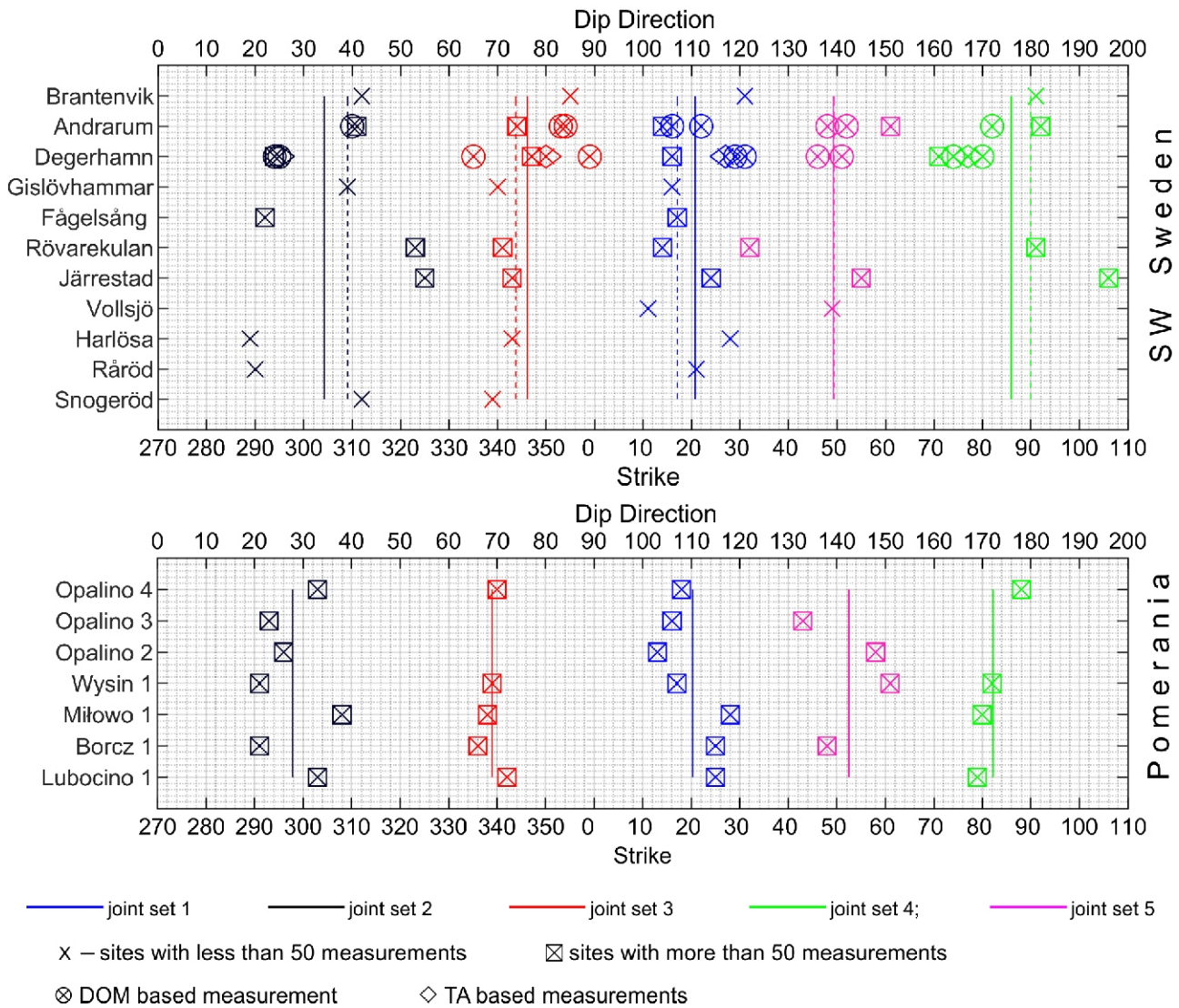


Fig. 9. Graphical comparison of all joint sets detected

Solid lines – mean orientation from all GC data; dashed lines – mean orientation from GC data with 50 and more measurements

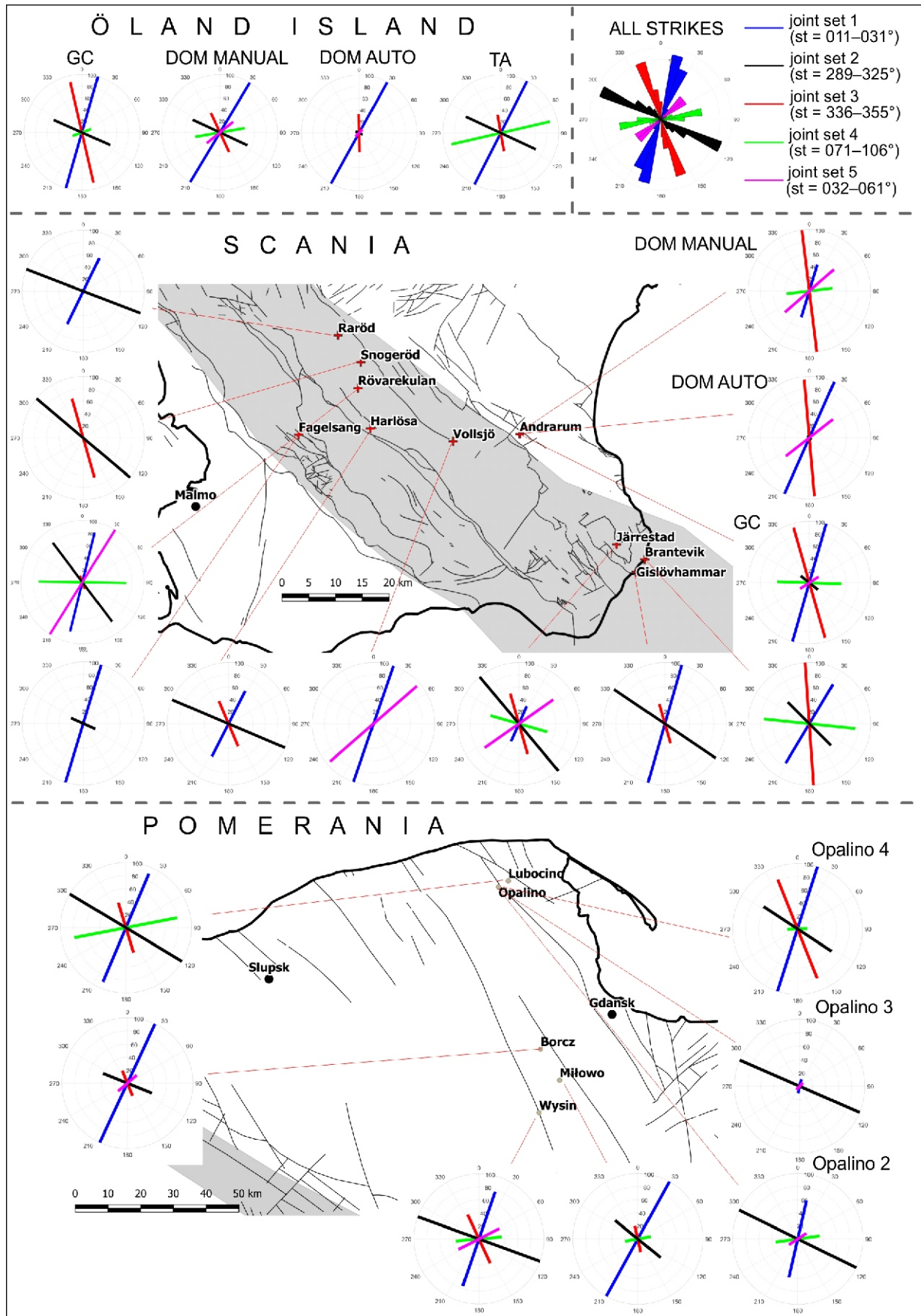


Fig. 10. Location maps with strike of the main joint sets

Line length in the strike diagrams is proportional to the percentage share of joint sets at a given location. Upper map – Scania region, background faults provided by the Geological Survey of Sweden via <https://www.sgu.se>. Lower map – Pomerania region, background faults provided by CBDG via ([http://geoportal.pgi.gov.pl/uslugi\\_gis](http://geoportal.pgi.gov.pl/uslugi_gis)), based on “Mapa geologiczna na poziomie ścięcia 3000 m p.p.m. na podstawie Atlasu Geologicznego Polski 1:750 000”

## DISCUSSION OF RESULTS

There are only 4 sites, spread over Scania, Öland, and E Pomerania, in which all five joint sets were observed. A large scatter in the direction of JS 2 and JS 4 suggests that they may be genetically heterogeneous and consist of smaller sub-sets. The best indicators of presumed block rotation are JS 1 and JS 3 due to their prevalence and directional stability across the Baltic Basin (Fig. 9). For instance, in the data from E Pomerania, a systematic rotation of joint sets from the mean is observed, e.g. in the Miłowo 1 borehole, where three major JSs (1, 2, 3) are noticeably rotated clockwise. A similar situation occurs in Opalino 3, but with the counter-clockwise rotation of all JSs (Fig. 9). Because both boreholes are located in an area where seismic-scale faults occur in the 3D seismic image (Bobek and Jarosiński, 2018), local palaeostress rotation in the vicinity of the faults is probably the reason for rotation of these joints.

The strike of JS 2, JS 4, and JS 3 in Scania seems to be rotated ~5–10° clockwise in relation to E Pomerania (Fig. 9). The orientations of JS 3 and JS 4 in data from Scania show much higher variance than in E Pomeranian data. A similar difference between different methods of joint detection (GC, TA and DOM) was observed in the exposures themselves. This suggests that the rotation of JS 4 is artificial or at least uncertain. In JS 3, apart from uncertain DOM measurements, the dispersion of data is much lower, but still 2–3 times larger than the difference between the mean orientation in Scania and E Pomerania, again suggesting an artificial origin of the observed change in its direction. JS 2 detected by different methods (DOM, GC and TA) in Degerhamn is consistent, but with highly spread directions between exposures across Scania, in contrast to E Pomerania where JS 2 has no strikes of 310° and higher. Joints oriented 310°+ are present in the Opalino 3, Opalino 2, Wysin 1, and Lubocino 1 boreholes, but in these cases, they were all treated as subordinates of JS 2, which may lead to an underestimation (apparent, counter-clockwise rotation) of strikes in the E Pomeranian data. The coherence of JS orientations in E Pomerania and SW Sweden is high, which suggests that the same basin-scale events were responsible for joint formation. This also suggests a lack of significant changes in stress directions across the region analysed.

East Pomerania and Öland are located at the boundary of the East European Craton, and so the occurrence of an identical joint pattern in both regions is understandable. Scania is located in a heavily faulted old shear zone, the Sorgenfrei-Tornquist Zone (STZ), thus here the presence of the same joint systems is less expected. Despite that in some cases the joint sets seem slightly rotated in the STZ relative to the more internal part of the craton, there are no major differences. The same JSs can be distinguished in both areas. Furthermore, when comparing the mean orientations of the joint sets in N Poland and Scania, which should minimize the influence of data bias, the observed rotation or changes in STZ are relatively small compared to the spread of orientations measured with different approaches for a single exposure, the same as for orientation spread within a single JS. Considering this, the JS rotation observed in the STZ should be treated with caution, and most of differences between E Pomerania and SW Sweden cannot be interpreted in terms of bending stress trajectory. There are no distinguishable, additional joint sets that could be generated by the separate STZ dynamics or present uplift of Scania. Since the presence of a dense fault network in STZ did not interfere with the development of joints, this suggests that the development of the entire joint system preceded the major phases of STZ tectonic activity which took place from the Permian to the Cretaceous, when several phases of subsi-

dence and erosion, accompanied by wrenching tectonics, have been distinguished (Erlstrom et al., 1997).

Due to observation spot (boreholes, unoriented core, weathered exposures) characteristics, no reliable observations of relative joint age were taken. The dating of the main jointing events suggested below is based on published palaeostress constraints. The first prerequisite for establishing a consistent joint set is burial at a depth where stable tectonic stresses may propagate efficiently in competent, compacted shale rock (English, 2012). The rapid subsidence of the research area began during and after the deposition of the Lower Silurian sequence, caused by plate bending in the foredeep basin of the Pomeranian Caledonides (Poprawa et al., 1999; Poprawa, 2019). After a short episode of minor erosion, subsidence most probably persisted in the Devonian (Matyja, 2006; Japsen et al., 2016; Botor et al., 2019). Considering that plate bending was the main tectonic subsidence mechanism for the entire Caledonian foreland, the better recognised trends in Poland can be extrapolated northwards. Due to the slightly more distal position of Scania than E Pomerania, with respect to the collision zone with Eastern Avalonia, relatively minor Silurian bending subsidence is expected for Scania.

According to apatite fission-track dating results (Japsen et al., 2016), the beginning of Scania's uplift and erosion after Variscan subsidence is dated to the latest Carboniferous (314–307 Ma), which is consistent with the models constructed for E Pomerania (Botor et al., 2019). In Scania, Variscan uplift might have been significant due to the strong magmatic event which most probably triggered the uplift of the Baltic Basin (Poprawa, 2019). Therefore, in the Permian, the Lower Paleozoic sequence is expected to be near the surface, conditions which were unfavourable for systematic joint development. Moreover, in late Variscan times, the Sorgenfrei-Tornquist Zone was active with dextral movements (Ziegler, 1992; McCann et al., 2006). At this time, the Lower Paleozoic sequence of Scania was heavily faulted by normal and strike-slip faults and subsequently involved in the pull-apart mechanism of local tectonic block subsidence. Early Permian wrenching was accompanied by a second episode of magmatism (Mogensen and Jensen, 1994) after the Carboniferous magmatic stage (Poprawa, 2019). From the above, it is inferred that after the tectonic disintegration of the Baltic Basin deposits in the Permian, there were no conditions favourable for the development of homogeneous joint sets. Therefore, the best time to develop a homogeneous joint system at the basin scale in the Lower Paleozoic shale sequence is the period from the late Silurian until the end of the Carboniferous. In this time interval the analysed complexes were buried under a thick cover of Silurian foredeep deposits, which became yet thicker in the Devonian.

Other necessary conditions for developing a regional joint set include a favourable stress regime and direction. The preferential stress and pressure conditions for the development of JS 1 and JS 2 in E Pomerania appeared probably in the late Carboniferous (McCann et al., 2006). Although the dataset analysed is not sufficient to constrain the details of joint development, an Early Devonian compressional stage in the Scandinavian Caledonides is proposed as a good candidate to trigger the origin of JS 3 and JS 4. This event was responsible for transpressive fault reactivation in the region studied (Poprawa et al., 1999), and the NNW trend of JS 3 well corresponds to the postulated direction of compression from this branch of the Caledonian orogen. The orthogonal JS 4 might have been created in the relaxation phase after this compressive event, which had to be accompanied by a significant change of stress regime and direction. Such an event has not yet been described. At the present stage of investigation of the Baltic Basin's tectonic evolution, there is no clear candidate for the origin of JS 5. Its poor

development and unstable orientation suggest a minor tectonic event responsible for triggering this joint set. A later, post-Paleozoic origin of JS 5 is also possible. Our concept of joint formation across the Baltic Basin is hypothetical and can serve as a background for more detailed analysis in the future.

## CONCLUSIONS

We integrate various methods of fracture orientation measurement, using direct observations on rock exposures, 3D imaging, trace analysis based on satellite imagery, and borehole logging interpretation using microresistivity imager data. The correlation between shale formations shows homogeneous facies and good lithostratigraphic continuity across the Baltic Basin, which was a foredeep basin of the North German-Polish Caledonides. These properties of basin infill may have favoured the effective stress propagation through shale formations necessary to develop wide-ranging joint sets. The Scania exposures are located in the Sorgenfrei-Tornquist Zone, while the Öland Island outcrops and the E Pomeranian boreholes are located in the interior of the East European Craton, less affected by Permian-Mesozoic tectonic events. The study shows that:

- the consistency of results obtained using different methods demonstrates that a multi-methodological approach can be successfully applied to joint pattern recognition;
- the resultant joint sets obtained from deep boreholes and outcrops of the Baltic Basin are similar, in terms of their orientation as well as showing their quantitative validity;
- in both E Pomerania and SW Sweden (Scania and Öland), five regional joint sets (JS 1 to JS 5) were distinguished: the most frequent is JS 1 with well-clustered

NNE orientation; a frequent but more scattered JS 2 trends WNW; the moderately developed and scattered JS 3 trends NNW; the subordinate JS 4 trends E–W with the largest angular spread of joint orientation seen in exposures; a subordinate JS 5 trends NE with moderate scattering;

- except for local, minor differences of mean joint directions for Scania and E Pomerania in the range of 10°, the consistency of joint set orientations observed is independent of the site location versus the Sorgenfrei-Tornquist Zone or craton interior.
- for consideration of hypothetical block rotations, or bending of the stress trajectory, the frequent and well-focused JS 1 and JS 3 may serve as a reference direction.

The orientations of JS 1 and JS 2 correspond to stress directions that occurred in the late Carboniferous, during the deep burial of the entire Lower Paleozoic sequence. It is hypothesised that the formation of JS 3 and JS 4 occurred in the early Devonian compressive stage and its relaxation. At the present stage of research, the origin of the less stable and poorly developed JS 5 is uncertain. From the point of view of fracture network analysis, the Lower Paleozoic strata in SW Sweden seem to be good analogues of buried E Pomeranian shale formations. The difference in uplift and erosion range between these two regions has limited impact on joint pattern.

**Acknowledgements.** The research has been done in the framework of the ShaleMech project funded by BlueGas – the Polish Shale Gas Programme of the National Centre for Research and Development (grant no. BG2/ShaleMech/14). The borehole data used was provided by the Polish Oil and Gas Company (PGNiG) from the ShaleMech project. The article was prepared with the support of Polish Geological Institute – National Research Institute project 62.9012.1958.00.0 funds.

## REFERENCES

- Assali, P., Grussenmeyer, P., Villemin, T., Pollet, N., Viguier, F., 2014.** Surveying and modeling of rock discontinuities by terrestrial laser scanning and photogrammetry: Semi-automatic approaches for linear outcrop inspection. *Journal of Structural Geology*, **66**: 102–114.
- Barton, C., Moos, D., 2010.** Geomechanical wellbore imaging: key to managing the asset life cycle. *AAPG Memoir*, **92**: 81–112.
- Barton, C.A., Zoback, M.D., 2002.** Discrimination of natural fractures from drilling-induced wellbore failures in wellbore image data – implications for reservoir permeability. *SPE Reservoir Evaluation & Engineering*, **5**: 249–254.
- Beier, H., Maletz, J., Bohnke, A., 2000.** Development of an Early Palaeozoic foreland basin at the SW margin of Baltica. *Neues Jahrbuch für Geologie und Paläontologie – Abhandlungen*, **218**: 129–152.
- Bellian, J.A., Kerans, C., Jennette, D.C., 2005.** Digital outcrop models: Applications of terrestrial scanning lidar technology in stratigraphic modeling. *Journal of Sedimentary Research*, **75**: 166–176.
- Bemis, S.P., Mickelthwaite, S., Turner, D., James, M.R., Akciz, S., Thiele, S.T., Bangash, H.A., 2014.** Ground-based and UAV-Based photogrammetry: a multi-scale, high-resolution mapping tool for structural geology and paleoseismology. *Journal of Structural Geology*, **69**: 163–178.
- Bergerat, F., Angelier, J., Andreasson, P.G., 2007.** Evolution of paleostress fields and brittle deformation of the Tornquist Zone in Scania (Sweden) during Permo-Mesozoic and Cenozoic times. *Tectonophysics*, **444**: 93–110.
- Bertrand, L., Géraud, Y., Le Garzic, E., Place, J., Diraison, M., Walter, B., Haffen, S., 2015.** A multiscale analysis of a fracture pattern in granite: A case study of the Tamaru granite, Catalunya, Spain. *Journal of Structural Geology*, **78**: 52–66.
- Bobek, K., Jarosiński, M., 2018.** Parallel structural interpretation of drill cores and microresistivity scanner images from gas-bearing shale (Baltic Basin, Poland). *Interpretation*, **6**: 25–38.
- Bobek, K., Jarosiński, M., 2021.** Modifications of methods for the fracture analysis from borehole data in application to shale formations. *Geological Quarterly*, **65**: 23.
- Bobek, K., Jarosinski, M., Pachtyel, R., 2017.** Tectonic Structures in Shale That You Do Not Include in Your Reservoir Model. 51st U.S. Rock Mechanics/Geomechanics Symposium, San Francisco, California, USA (<https://onepetro.org/ARMAUSRMS/proceedings-abstract/ARMA17/All-ARMA17/ARMA-2017-0079/126475>)
- Botor, D., Golonka, J., Anczkiewicz, A., Dunkl, I., Papiernik, B., Zając, J., Guzy, P., 2019.** Burial and thermal history of the Lower Palaeozoic petroleum source rocks at the SW margin of the East European Craton (Poland). *Annales Societatis Geologorum Poloniae*, **89**: 121–152.
- Brudy, M., Zoback, M.D., 1999.** Drilling-induced tensile wall-fractures: implications for determination of in-situ stress orientation and magnitude. *International Journal of Rock Mechanics and Mining Sciences*, **36**: 191–215.

- Buckley, S.J., Howell, J.A., Enge, H.D., Kurz, T.H., 2008.** Terrestrial laser scanning in geology: data acquisition, processing and accuracy considerations. *Journal of the Geological Society*, **165**: 625–638.
- Calner, M., Ahlberg, P., Lehnert, O., Erlström, M., 2013.** The Lower Palaeozoic of southern Sweden and the Oslo Region, Norway. Field Guide for the 3rd Annual Meeting of the IGCP project 591. Sveriges geologiska undersökning Rapport och meddelanden, **133**: 96, <https://lup.lub.lu.se/search/publication/13500fdc-e5e0-4a78-9f3d-d32bc2159f86>
- Cignoni, P., Callieri, M., Corsini, M., Dellepiane, M., Ganovelli, F., Ranzuglia, G., 2008.** MeshLab: an Open-Source Mesh Processing Tool. Eurographics Italian Chapter Conference 2008, Salerno, Italy: 129–136
- CloudCompare**, [www.danielgm.net/cc/](http://www.danielgm.net/cc/), access: 02.03.2020.
- Cocks, L.R.M., Torsvik, T.H., 2005.** Baltica from the late Precambrian to mid-Palaeozoic times: the gain and loss of a terrane's identity. *Earth-Science Reviews*, **72**: 39–66.
- Corradetti, A., Tavani, S., Russo, M., Arbues, P.C., Granado, P., 2017.** Quantitative analysis of folds by means of orthorectified photogrammetric 3D models: a case study from Mt. Catria, Northern Apennines, Italy. *Photogrammetric Record*, **32**: 480–496.
- Dewez, T.J.B., Girardeau-Montaut, D., Allanic, C., Rohmer, J., 2016.** Facets: a Cloudcompare Plugin to Extract Geological Planes from Unstructured 3d Point Clouds. XXIII ISPRS Congress, Commission V: 799–804, <https://doi.org/10.5194/isprs-archives-XLI-B5-799-2016>
- Enge, H.D., Buckley, S.J., Rotevatn, A., Howell, J.A., 2007.** From outcrop to reservoir simulation model: Workflow and procedures. *Geosphere*, **3**: 469–490.
- Engelder, T., Lash, G.G., Uzcátegui, R.S., 2009.** Joint sets that enhance production from Middle and Upper Devonian gas shales of the Appalachian Basin. *AAPG Bulletin*, **93**: 857–889.
- Engelder, T., Slingerland, R., Arthur, M., Lash, G., Kohl, D., Gold, D.P., 2011.** An introduction to structures and stratigraphy in the proximal portion of the Middle Devonian Marcellus and Burket/Geneseo black shales in the Central Appalachian Valley and Ridge. From the Shield to the Sea: Geological Field Trips from the 2011 Joint Meeting of the GSA Northeastern and North-Central Sections: 17–44, [https://doi.org/10.1130/2011.0020\(02\)](https://doi.org/10.1130/2011.0020(02)).
- English, J.M., 2012.** Thermomechanical origin of regional fracture systems. *AAPG Bulletin*, **96**: 1597–1625.
- Erlström, M., 2020.** Carboniferous–Neogene tectonic evolution of the Fennoscandian transition zone, southern Sweden. *Geological Society, London, Memoirs*, **50**: 603–620.
- Erlstrom, M., Thomas, S.A., Deeks, N., Sivhed, U., 1997.** Structure and tectonic evolution of the Tornquist Zone and adjacent sedimentary basins in Scania and the southern Baltic Sea area. *Tectonophysics*, **271**: 191–215.
- Franke, D., 1993.** The southern border of Baltica – a review of the present state of knowledge. *Precambrian Research*, **64**: 419–430.
- Furukawa, Y., Ponce, J., 2010.** Accurate, dense and robust multiview stereopsis. *IEEE Transactions on Pattern Analysis and Machine Intelligence*, **32**: 1362–1376.
- Gale, J.F.W., Laubach, S.E., Olson, J.E., Eichhuble, P., Fall, A., 2014.** Natural fractures in shale: a review and new observations. *AAPG Bulletin*, **98**: 2165–2216.
- GoogleEarth**, <https://www.google.com/earth/>, access: 07.07.2020.
- Hansen, D.L., Nielsen, S.B., Lykke-Andersen, H., 2000.** The post-Triassic evolution of the Sorgenfrei-Tornquist Zone – results from thermo-mechanical modelling. *Tectonophysics*, **328**: 245–267.
- Hill, D., Lombardi, T., Martin, J., 2004.** Fractured shale gas potential in New York. *Northeastern Geology and Environmental Sciences*, **26**: 57–78.
- Japsen, P., Green, P.F., Bonow, J.M., Erlstrom, M., 2016.** Episodic burial and exhumation of the southern Baltic Shield: epeirogenic uplifts during and after break-up of Pangaea. *Gondwana Research*, **35**: 357–377.
- Jebara, T., Azarbajehani, A., Pentland, A., 1999.** 3D structure from 2D motion. *IEEE Signal Processing Magazine*, **16**: 66–84.
- Jordá Bordehore, L., Riquelme, A., Cano, M., Tomás, R., 2017.** Comparing manual and remote sensing field discontinuity collection used in kinematic stability assessment of failed rock slopes. *International Journal of Rock Mechanics and Mining Sciences*, **97**: 24–32.
- Klawitter, M., Pistellato, D., Webster, A., Esterle, J., 2017.** Application of photogrammetry for mapping of solution collapse breccia pipes on the Colorado Plateau, USA. *Photogrammetric Record*, **32**: 443–458.
- Le Garzic, E., de L'Hamaide, T., Diraison, M., Géraud, Y., Sausse, J., de Urreiztieta, M., Hauville, B., Champanhet, J.-M., 2011.** Scaling and geometric properties of extensional fracture systems in the proterozoic basement of Yemen. Tectonic interpretation and fluid flow implications. *Journal of Structural Geology*, **33**: 519–536.
- Matyja, H., 2006.** Stratigraphy and facies development of Devonian and Carboniferous deposits in the Pomeranian Basin and in the western part of the Baltic Basin and palaeogeography of the northern TESZ during Late Palaeozoic times (in Polish with English summary). *Prace Państwowego Instytutu Geologicznego*, **186**: 79–122.
- Mazur, S., Mikołajczak, M., Krzywiec, P., Malinowski, M., Buffenmyer, V., Lewandowski, M., 2015.** Is the Teisseyre-Tornquist Zone an ancient plate boundary of Baltica? *Tectonics*, **34**: 2465–2477.
- Mazur, S., Aleksandrowski, P., Gągała, Ł., Krzywiec, P., Żaba, J., Gaidzik, K., Sikora, R., 2020.** Late Palaeozoic strike-slip tectonics versus oroclinal bending at the SW outskirts of Baltica: case of the Variscan belt's eastern end in Poland. *International Journal of Earth Sciences*, **109**: 1133–1160.
- McCann, T., Pascal, C., Timmerman, M.J., Krzywiec, P., López-Gómez, J., Wetzel, L., Krawczyk, C.M., Rieke, H., Lamarche, J., 2006.** Post-Variscan (end Carboniferous–Early Permian) basin evolution in Western and Central Europe. *Geological Society, Memoirs*, **32**: 355–388.
- Mehlqvist, K., Steemans, P., Vajda, V., 2015.** First evidence of Devonian strata in Sweden – a palynological investigation of Övedskloster drillcores 1 and 2, Skåne, Sweden. *Review of Palaeobotany and Palynology*, **221**: 144–159.
- Menegoni, N., Meisina, C., Perotti, C., Crozi, M., 2018.** Analysis by UAV digital photogrammetry of folds and related fractures in the Monte Antola Flysch Formation (Ponte Organasco, Italy). *Geosciences*, **8**: 299.
- Modliński, Z., Podhalańska, T., 2010.** Outline of the lithology and depositional features of the lower Paleozoic strata in the Polish part of the Baltic region. *Geological Quarterly*, **54** (2): 109–121.
- Mogensen, T.E., Jensen, L.N., 1994.** Cretaceous subsidence and inversion along the Tornquist Zone from Kattegat to the Egersund Basin. *First Break*, **12**: 211–222.
- Nie, X., Zou, C., Pan, L., Huang, Z., Liu, D., 2013.** Fracture analysis and determination of in-situ stress direction from resistivity and acoustic image logs and core data in the Wenchuan Earthquake Fault Scientific Drilling Borehole-2 (50–1370 m). *Tectonophysics*, **593**: 161–171.
- Nielsen, A.T., 1995.** Trilobite systematics, biostratigraphy and palaeoecology of the Lower Ordovician Komstad Limestone and Huk Formations, southern Scandinavia. *Fossils and Strata*, **38**: 374.
- Osborne, M., J., Swarbrick, R., E., 1997.** Mechanisms for generating overpressure in sedimentary basins: a reevaluation. *AAPG Bulletin*, **81**: 1023–1041.
- Poprawa, P., 2019.** Geological setting and Ediacaran–Palaeozoic evolution of the western slope of the East European Craton and adjacent regions. *Annales Societatis Geologorum Poloniae*, **89**: 47–80.
- Poprawa, P., Śliupa, S., Stephenson, R., Lazauskienė, J., 1999.** Late Vendian–Early Paleozoic tectonic evolution of the Baltic Basin: regional tectonic implications from subsidence analysis. *Tectonophysics*, **314**: 219–239.

- Samsu, A., Cruden, A.R., Micklethwaite, S., Grose, L., Vollgger, S.A., 2020.** Scale matters: the influence of structural inheritance on fracture patterns. *Journal of Structural Geology*, **130**: 103896.
- Sturzenegger, M., Stead, D., 2009.** Close-range terrestrial digital photogrammetry and terrestrial laser scanning for discontinuity characterization on rock cuts. *Engineering Geology*, **106**: 163–182.
- Thiele, S.T., Grose, L., Samsu, A., Micklethwaite, S., Vollgger, S.A., Cruden, A.R., 2017.** Rapid, semi-automatic fracture and contact mapping for point clouds, images and geophysical data. *Solid Earth*, **8**: 1241–1253.
- Thybo, H., 1997.** Geophysical characteristics of the Tornquist Fan area, northwest Trans-European Suture Zone: indication of late Carboniferous to early Permian dextral transtension. *Geological Magazine*, **134**: 597–606.
- Voigt, T., Kley, J., Voigt, S., 2021.** Dawn and dusk of Late Cretaceous basin inversion in central Europe. *Solid Earth*, **12**: 1443–1471.
- Westoby, M.J., Brasington, J., Glasser, N.F., Hambrey, M.J., Reynolds, J.M., 2012.** ‘Structure-from-Motion’ photogrammetry: a low-cost, effective tool for geoscience applications. *Geomorphology*, **179**: 300–314.
- Wu, C., SiftGPU: A GPU implementation of scale invariant feature transform (SIFT)**, <http://cs.unc.edu/~ccwu/siftgpu>, access: 23.02.2017.
- Wu, C., Agarwal, S., Curless, B., Seitz, S.M., 2011.** Multicore bundle adjustment. *Proceedings of the IEEE Conference on Computer Vision and Pattern Recognition*, Colorado Springs, CO, USA: 3057–3064
- Ziegler, P.A., 1992.** *Geological Atlas of Western and Central Europe* (2nd Edition). Geological Society of London, London.
- Zoback, M.D., Kohli, A.H., 2019.** *Unconventional Reservoir Geomechanics: Shale Gas, Tight Oil, and Induced Seismicity*. Cambridge University Press, Cambridge.